Material Recognition from Heat Transfer given Varying Initial Conditions and Short-Duration Contact

Tapomayukh Bhattacharjee, Joshua Wade, and Charles C. Kemp
Healthcare Robotics Lab, Institute for Robotics and Intelligent Machines, Georgia Institute of Technology, Atlanta, Georgia 30308
Email: {tapomayukh, josh_wade}@gatech.edu, charlie.kemp@bme.gatech.edu

***Abstract*—When making contact with an object, a robot can use a tactile sensor consisting of a heating element and a temperature sensor to recognize the object's material based on conductive heat transfer from the tactile sensor to the object. When this type of tactile sensor has time to fully reheat prior to contact and the duration of contact is long enough to achieve a thermal steady state, numerous methods have been shown to perform well. In order to enable robots to more efficiently sense their environments and take advantage of brief contact events over which they lack control, we focus on the problem of material recognition from heat transfer given varying initial conditions and short-duration contact. We present both model-based and data-driven methods. For the model-based method, we modeled the thermodynamics of the sensor in contact with a material as contact between two semi-infinite solids. For the data-driven methods, we used three machine learning algorithms (SVM+PCA, k-NN+PCA, HMMs) with time series of raw temperature measurements and temperature change estimates. When recognizing 11 materials with varying initial conditions and 3-fold cross-validation, SVM+PCA outperformed all other methods, achieving 84% accuracy with 0.5 s of contact and 98% accuracy with 1.5 s of contact.**

I. Introduction

When a robot's body makes physical contact with the world, it has a distinct opportunity to sense its surroundings. Multimodal tactile sensors can combine a variety of types of sensing, such as pressure, vibration, and temperature sensing, each with its own capabilities and limitations. Tactile sensing based on conductive heat transfer can be highly informative about materials in contact with the robot, but has temporal limitations. In order for heat to flow from the sensor to a material, the sensor is typically heated prior to contact and then held in contact with the material. The resulting temperature measurements over time can then be used to recognize the material. For example, touching an aluminum object results in a rapid drop in temperature as heat flows into the aluminum (see Fig. 1), which is related to the cold sensation a person feels upon touching aluminum at room temperature.

When a tactile sensor has time to achieve a consistent temperature well above the ambient temperature of the environment and stays in contact with an object until it reaches a thermal steady state, many methods can recognize the material with good performance. However, these requirements greatly decrease the temporal efficiency of tactile sensing, since they reduce the rate at which a sensor can make contact with the world and require that the sensor be held in contact for a substantial length of time. In this paper, we focus on the problem of recognizing materials given short-duration contact and varying initial conditions, which results in visibly different temperature time series, as seen in Fig. 1.

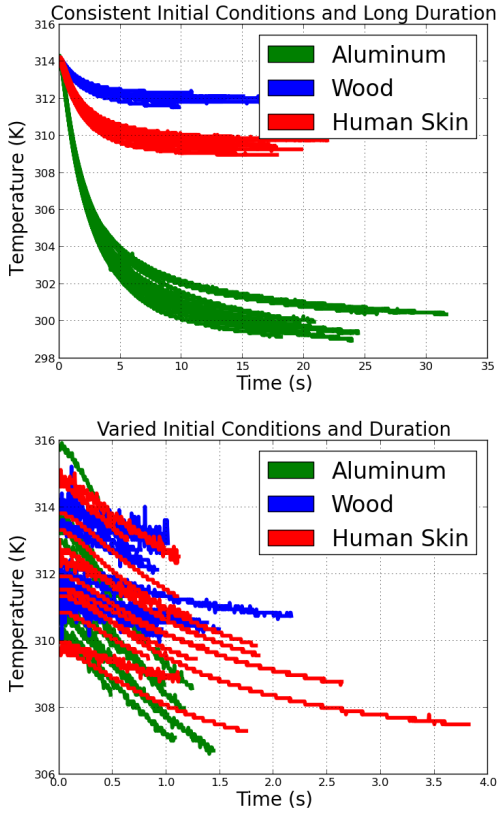

Fig. 1: *Example temperature features for robot experiments with a) consistent initial conditions and long duration (top), b) varied initial conditions and duration (bottom).*

Many robotics applications would benefit from methods that recognize materials from short-duration contact with less time between contact events. In general, this would increase the speed at which a robot acquires information using touch. As we discuss later, recent algorithm-centric research on heat-transfer-based sensing has used contact durations of 15 s or longer and consistent initial conditions. In contrast, we show the feasibility of acquiring useful information 30x faster with 0.5 s of contact, initial sensor temperatures varying from 26°C to 40°C in a room with an ambient temperature of 25°C, and

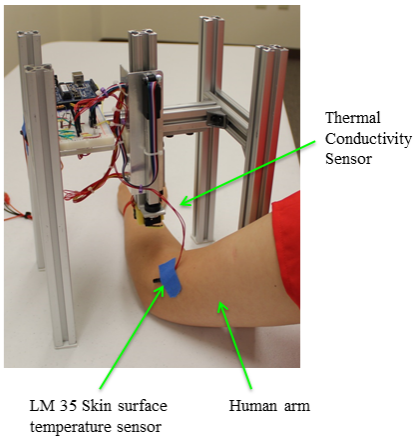

Fig. 2: *Experimental setup with a 1-DOF linear actuator to measure thermal response of different materials in contact.*

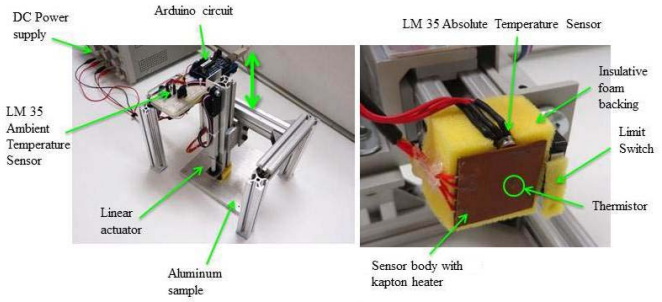

Fig. 3: *Sensor test rig composed of a) linear actuator, Arduino circuit and sensor (left), b) Heat-transfer-based tactile sensor with a single-sided transient plane source technique (right).*

materials that did not fully cool down to the ambient temperature between contact events. This is a markedly different level of efficiency and opens up the possibility of new uses for sensing based on heat transfer, such as helping a robot find metal keys in a bag.

The potential for robots to acquire information from incidental contact between their bodies and their surroundings has motivated our work. By *incidental contact*, we mean contact that is not central to the robot's current actions and may occur unexpectedly or unintentionally [1, 2]. In contrast to deliberate probing during which the robot controls contact to improve perception, sensing during incidental contact is opportunistic with the robot inferring what it can from contact as it occurs. For example, a robot reaching into a densely cluttered environment can use tactile sensing across its arm to better maneuver within the environment and map it [1, 2]. Likewise, an assistive robot reaching around a person with disabilities could potentially use tactile sensing to recognize contact between its arm and the person's body or wheelchair [3]. Similarly, tactile sensing across a robot's fingers might provide useful information during in-hand manipulation. All of these tasks could potentially benefit from tactile sensing based on heat transfer, but would be sensitive to the temporal limitations we address in this paper.

II. Related Work

Many researchers have used thermal sensing in studies with consistent initial conditions and long duration contact using specialized exploratory behaviors. In contrast to these studies, our work focuses on short-duration contact (without reaching steady-state) with varying initial conditions. Also, instead of investigating multiple sensory modalities, we focus on the performance of heat-transfer-based sensing in isolation. Unlike most previous studies, we have developed a physics-based model for material recognition for increased understanding of the recognition problem and to provide a comparison with data-driven methods.

A. Short-duration Contact with Consistent Initial Conditions

Studies in this section focus on thermal sensing during short-duration contact. However, these studies are hardware-centric with limited evaluation. In addition, all of these studies use methods that assume consistent initial conditions.

1) Hardware-centric: Russell [4, 5] developed a thermal sensing array with which he compared the percent decrease in temperature from a uniform initial temperature after 3 s of contact. The array successfully recognized six distinct materials in a single trial [4, 5]. Siegal *et al.* [6] developed another sensor with a slower temporal response, according to Monkman and Taylor [7]. Monkman and Taylor [7] developed two methods of thermal sensing that they reported to be faster than Russell's or Siegal *et al.*'s . One sensor used a Peltier heating element, and the other used a pyrometer and a heating element. They evaluated the two sensors with respect to the recognition of four materials with distinct thermal properties given consistent initial conditions. Their figure showing sensor readings over time from a single trial with each material, suggests that recognition of these four materials could potentially be performed quickly (between 0 s and 3 s), but they did not report specific results. Engel *et al.* [8, 9] developed a flexible multimodal tactile sensing system that included a side-by-side gold heater and temperature sensor. Based on combined pressure and thermal sensing, their system recognized 5 materials with 90% accuracy over 50 trials with consistent initial conditions, but unreported contact duration. Our methods could potentially be used with these and other sensors that use heat transfer, and different hardware might result in improved performance.

B. Long-duration Contact with Consistent Initial Conditions

Studies in this section deal with thermal sensing under idealized scenarios with consistent initial conditions and long-duration contact.

1) Hardware-centric: Many researchers have included thermal sensing as a part of multimodal tactile sensing hardware, such as absolute temperature sensors [10], [11] and sensors that use heat transfer [12], [13], [14], [15], [16]. However,

this body of work focuses on hardware development with little evaluation of material recognition performance.

2) Algorithm-centric: A number of researchers have performed algorithm-centric research using existing sensor hardware to perform tasks related to material recognition. Xu *et al.* [17] used a Syntouch BioTAC sensor to measure the temperature derivative during 15 s of contact using exploratory behaviors from Bayesian exploration coupled with Reinforcement Learning techniques. They used multimodal sensor data to identify 10 objects with 99% accuracy [17]. McMahon *et al.* [18] used HMMs to automatically assign adjectives to haptic signals collected from a BioTAC sensor using approximately 80 s of data. [18]. Takamuku *et al.* [19] constructed a soft anthropomorphic finger that included both tactile and thermal sensors. They achieved classification by recording the convergent temperatures of 5 materials after 35 s of contact [19]. Kerr *et al.* [20] also used a heated BioTAC sensor (allowed 15-20 minutes to reach a steady-state after it is powered on) to record the thermal response data of 6 material groups with varying thermal properties for 20 s. They used the static temperature (TAC) and dynamic thermal conductivity (TDC) data from 15 trials for each material and implemented ANN with 73% accuracy [20].

In summary, the above studies focus on long-duration contact with consistent initial conditions using specific exploratory behaviors. Hardware-centric studies have focused on designing new thermal sensors with limited material recognition evaluation, while algorithm-centric studies have focused on data-driven algorithms such as HMMs, ANNs, and other ML-based methods. Most of the studies have used results from multimodal sensing devices, obscuring the role of thermal sensing.

III. Experiments

A. Experimental Setup

Figure 3 shows the test rig we used in our experiments. We constructed our sensor from the Thorlabs HT10K Foil Heater/Thermistor [21] which contains a 20 Ω heater and a 10 kΩ NTC thermistor. Our sensing technique is based on the single-sided transient plane source method that Mathis *et al.* [22] developed for characterizing samples of materials. This material characterization typically involves estimating material properties, such as thermal effusivity and thermal conductivity, for use in industrial applications, such as monitoring the quality of products, for which initial conditions can be controlled and the duration of contact can be long [12]. In contrast to previous transient plane source methods that required a sensor to be sandwiched between two samples of the material [23], [24], the single-sided approach [22] only requires that the sensor make frontal contact with a sample of the material, making it appropriate for tactile sensors that cover a robot. For this approach, the heater and temperature sensor are on a thermally insulating backing.

In general, a higher initial sensor temperature corresponds to better quality data. We chose a sensor heater supply voltage of 2.5 volts, so that a person can comfortably touch the sensor surface. We mounted the sensor on a layer of thermally insulating foam with the front face exposed as seen in Fig. 3. When the warmed sensor is brought into contact with an unknown surface, heat transfer from the sensor to the material occurs at a rate that depends on the material's temperature, thermal conductivity, density and specific heat capacity. We also installed a separate LM35 Precision Centigrade Temperature Sensor to measure the heater temperature and a limit switch to detect contact with the material and support autonomous data collection. To measure the ambient temperature of the room, we added a second LM35 temperature sensor on top of the test rig.

The test rig shown in Fig. 3 uses a 1-DOF linear actuator to move the heat-transfer-based tactile sensor. All sensors and actuators are connected to an Arduino Duemilanove. We used a DC power supply to run the linear actuator and sensor heater.

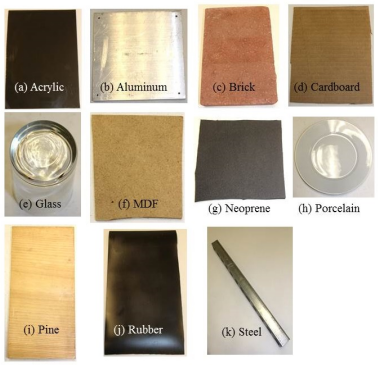

Fig. 4: *Material test set consisting of a) Acrylic, b) Aluminum, c) Brick, d) Cardboard, e) Glass, f) Medium-density fiberboard (MDF), g) Neoprene, h) Porcelain, i) pine wood, j) Rubber, k) Steel. Please note that we have a separate subsection that analyzes the tests with a human forearm (Section VII-E).*

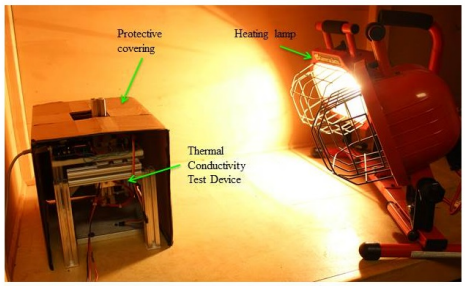

Fig. 5: *Warm environment test configuration. We used a heating lamp as a heat source along with a protective covering to avoid direct thermal radiation from the lamp and provide an isolated environment for the experiments.*

B. Experimental Procedure

Figure 3 demonstrates the use of the test rig to sense an aluminum sample. We used a Python script running on a separate computer to control the device through a serial link with the Arduino. Before contacting the sample, the device

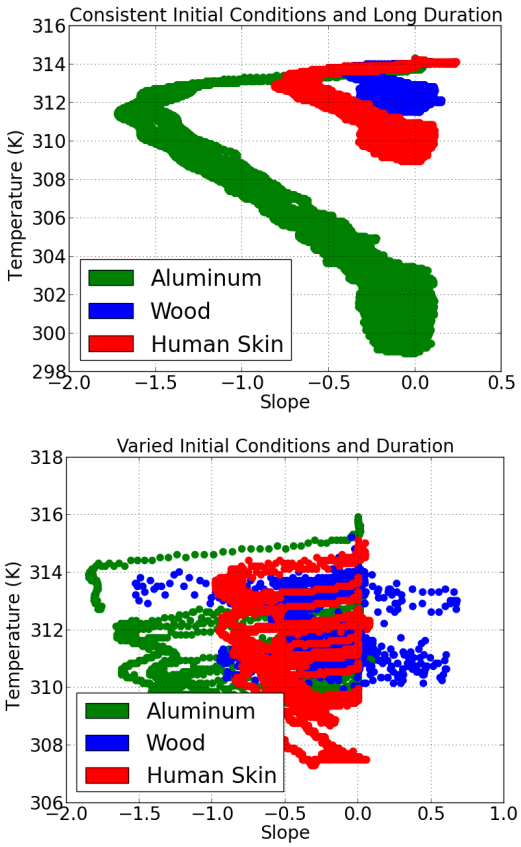

Fig. 6: *Example temperature and slope features for experiments with a) consistent initial conditions and long duration (top), b) varied initial conditions and duration (bottom).*

waited with the linear actuator in the "Up" position and allowed the heating element to heat the sensor body. Once heated, the device lowered the linear actuator and brought the heat-transfer-based tactile sensor in contact with the unknown sample. As the two bodies came to a thermal steady state, the Arduino recorded the thermistor, ambient temperature sensor and absolute temperature sensor outputs at 200 Hz. We programmed the device to be in contact with the sample until the thermistor temperature maintained a constant value for 3 s or a total of 35 s passed. We truncated these trials in time to simulate different durations of contact. Once a trial was completed, the device raised the linear actuator and waited for the sensor body to reheat before making contact with the material again.

To gather data with varying initial conditions, we randomized the reheat time with each trial to be in the range of 2-60 s. After every 10 trials, the device waited for 10 minutes with the sensor in the "Up" position to allow the test sample to cool and the sensor to fully reheat. This method generated trials with the initial sensor temperatures distributed in the range of 26-40°C in a room that was at 25°C.

C. Data Collection

Figure 1 shows the temperature data from various trials with samples of aluminum and wood, as well as a human forearm. As seen in the figure, materials with different thermal properties exhibit distinct temperature time series that vary based on the initial conditions. Despite this variation, features of the temperature time series remain similar for a given material.

Figure 4 shows the set of 11 test materials with various thermal properties that we used in our experiments. We collected 500 trials with random initial conditions for each material using the automated test rig shown in Fig. 3, giving a total of 5500 trials. During the experiment, we maintained the room temperature at 25°C throughout the day. The sensor temperature during this set of experiments varied from 26°C minimum to 40°C maximum with an average of 30°C across all the trials just before contact. To investigate the role of ambient temperature on performance, we conducted a second set of experiments in a warm environment of 35°C as shown in Fig. 5. We used a heating lamp to heat the surroundings to 35°C and a protective covering to isolate the sample. For this set, the sensor temperature varied from 35°C minimum to 43°C maximum with an average of 37°C across all the trials just before contact. We collected an additional 500 trials with random initial conditions for both aluminum and pine wood in the warm environment, resulting in 1000 total trials. We also collected two more data sets that we describe in Sections VII-B and VII-E.

D. Data Preprocessing and Feature Extraction

For each trial in an experiment, we collected the thermistor raw analog values at 200 Hz. We truncated the data at the onset of contact and obtained time-series vectors until steady-state was reached. To simulate varying contact duration, we used the first 0.5-2.5 s of data after the onset of contact. Fig. 1 shows the raw temperature time series for three example materials. In addition to the raw temperatures, our methods used estimates of the the derivative (slope) of the temperature with respect to time by taking the first difference of the raw signals and then using a causal filter. The filter was an 8th-order digital low-pass Butterworth filter with Nyquist frequency of 100 Hz and cutoff frequency of 2 Hz. Fig. 6 shows the slope features.

IV. Modeling Heat Transfer

We modeled the heat transfer between the heat-transfer-based tactile sensor and a block of material as contact between two semi-infinite solids, which we refer to as the sensor body and the object body [12, 25]. Fig. 7 shows a diagram representing the model. A semi-infinite solid is an idealized body for which the temperature change in a part of the body is due to thermal conditions on a single surface [25]. In an analogous manner, [25] has modeled a finger touching a material as a contact between two semi-infinite bodies.

First, we assume that the initial temperature of the object body, $T_{obj(t=0)}$, is constant throughout its extent and equal to the ambient temperature, T_{amb}.

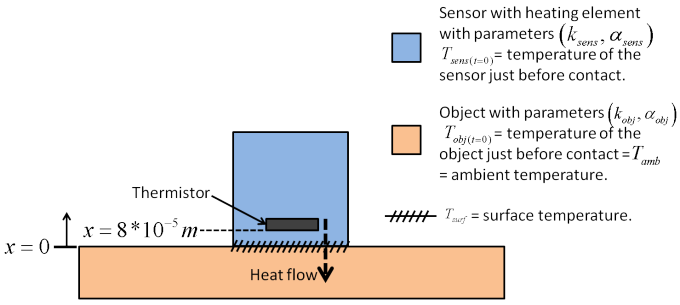

Fig. 7: *Diagram representing our model of the sensor in contact with a material. We model both bodies as semi-infinite solids.*

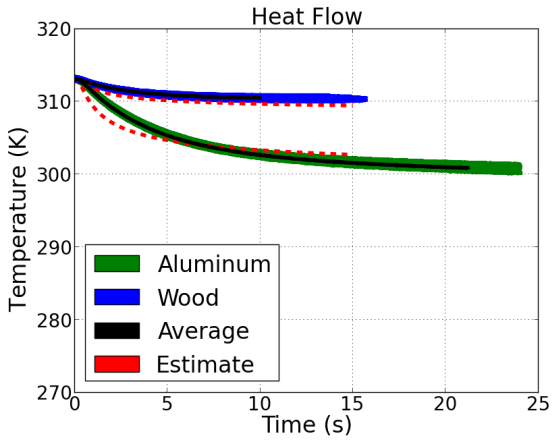

Fig. 8: *Forward simulation results for pine wood and aluminum with temperature values.*

Second, we find the initial temperature of the sensor body, $T_{sens(t=0)}$. The input to the sensor body is the heat flux, $\dot{q}_x$, from the electrical heating element given by

$$\dot{q}_x = \frac{V^2}{R} \tag{1}$$

where V is the supply voltage, and R is the resistance of the heating element. $T_{sens(t=0)}$ is constant across the entire sensor body and results from the heating element heating the sensor body before it comes into contact with the object body (i.e., the material sample). We find $T_{sens(t=0)}$ using Fourier's law of Heat Conduction [25],

$$\frac{\dot{q}_x}{A} = k_{sens}\frac{T_{sens(t=0)} - T_{amb}}{l} \tag{2}$$

where A is the cross-sectional area of the heating element, l is the height of the sensor body (i.e., length in x dimension), T_{amb} is the ambient temperature, k_{sens} is the coefficient of thermal conductivity of the sensor body, and $\frac{\dot{q}_x}{A}$ is the magnitude of heat flux per unit cross-sectional area.

Once the sensor body comes into contact with the object body, heat begins to flow from the sensor body to the object body and the temperature varies with time and position. When the bodies come into contact with one another, the surface between them at $x = 0$ (see Fig. 7) attains a temperature, T_{surf}, that remains constant throughout the duration of contact and is given by

$$T_{surf} = \frac{\left(T_{sens(t=0)}\frac{k_{sens}}{\sqrt{\alpha_{sens}}} + T_{obj(t=0)}\frac{k_{obj}}{\sqrt{\alpha_{obj}}}\right)}{\left(\frac{k_{sens}}{\sqrt{\alpha_{sens}}} + \frac{k_{obj}}{\sqrt{\alpha_{obj}}}\right)} \tag{3}$$

where α_{obj} and k_{obj} are the coefficients of thermal diffusivity and thermal conductivity of the object body, and α_{sens} and k_{sens} are the coefficients of thermal diffusivity and thermal conductivity of the sensor body.

Once we have found $T_{sens(t=0)}$ and T_{surf}, we can find the temperature in the sensor body at any time, $t >= 0$, using the following partial differential equation from [25]:

$$\frac{\partial^2 T_{sens}}{\partial x^2} = \frac{1}{\alpha_{sens}}\frac{\partial T_{sens}}{\partial t} \tag{4}$$

where $T_{sens}(x,t)$ is the temperature at time t of the sensor body at distance x from the surface between the two bodies. The thermistor, which is inside the sensor body, measures the temperature $T_{sens}(x = 8*10^{-5}, t)$ (see Fig. 7). Using our boundary conditions, $T_{sens}(x = 0, t) = T_{surf}$and $T_{sens}(x, t = 0) = T_{sens(t=0)}$ we can solve for $T_{sens}(x,t)$.

$$T_{sens}(x,t) = T_{sens(t=0)} + \left(T_{surf} - T_{sens(t=0)}\right) * erfc\left(\frac{x}{2\sqrt{\alpha_{sens} t}}\right) \tag{5}$$

where $erfc()$ is the complimentary error function given by

$$erfc(z) = \frac{2}{\sqrt{\pi}}\int_z^\infty e^{-r^2} dr \tag{6}$$

With this forward model we can predict the sensor readings, $T_{sens}(x = 8*10^{-5}, t)$, that would result from the heat-transfer-based tactile sensor coming into contact with a material with coefficient of thermal diffusivity α_{obj} and thermal conductivity k_{obj}.

V. Simulation Results

A. Forward Simulation

We used the heat-transfer model from Section IV to simulate the temperature measurements, $T_{sens}(x = 8*10^{-5}, t)$, that would result from our sensor coming into contact with a known object, specifically a block of pine wood or a block of aluminum. We used the coefficients of thermal conductivity and diffusivity, $k_{obj}$and α_{obj}, for pine wood and aluminum from the CES materials database [26]. For aluminum, $\alpha_{obj} = 3.55 * 10^{-5}\ m^2/s$ and $k_{obj} = 80\ W/(mK)$ and for pine wood, $\alpha_{obj} = 2.05 * 10^{-7}\ m^2/s$ and $k_{obj} = 0.15\ W/(mK)$. We obtained the cross-sectional area of the heating element $A = 1.5625 * 10^{-4}\ m^2$, the height $l = 2.4 * 10^{-4}\ m$ and the thermistor location at a distance $x = 8 * 10^{-5}\ m$ from the sensor data sheet [21]. We calculated the heat flux using eq. (1) with $V = 2.5$ volt and $R = 19.7\ \Omega$. We set the

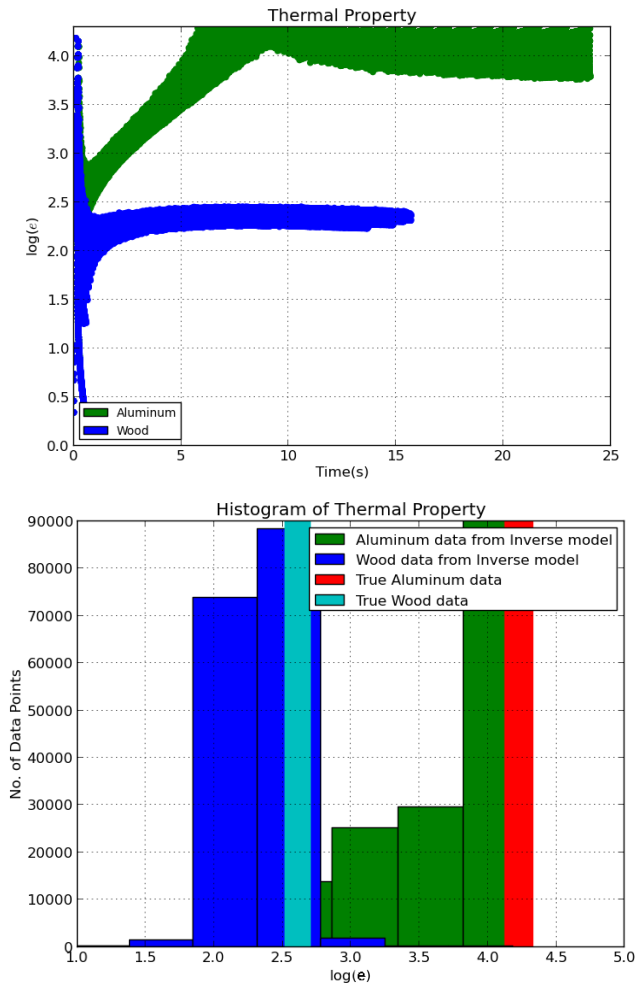

Fig. 9: *Inverse Simulation of the heat-transfer data (top), Histogram of the thermal property (bottom). Shaded regions in the histogram show the true values.*

initial temperature of the material $T_{obj(t=0)}$ to be the ambient temperature, 25 °C.

We calibrated the tactile sensor's thermistor using a simplified version of the standard Steinhart-Hart equation [27],

$$T = \frac{1}{C_1 ln(R_{th}) + C_0}, \tag{7}$$

which relates the absolute temperature, T, to the resistance across the thermistor, R_{th}. Our calibration resulted in $C_0 = 9.5594 * 10^{-4}$ and $C_1 = 2.6181 * 10^{-4}$. A resistive voltage divider with the thermistor, R_{th}, and a resistor, R_{REF}, performed the only signal conditioning prior to analog-to-digital (A/D) conversion by an Arduino Duemilanove board. The A/D converter linearly converted a 0-1.1 volt analog signal to a 10-bit digital signal, A_{in}.

$$R_{th} = R_{REF}[\frac{V^+}{\frac{A_{in}}{1023}V_{REF}} - 1] \tag{8}$$

relates R_{th} to A_{in} with $R_{REF} = 668\ \Omega$, $V^+ = 5.06$ volts, and $V_{REF} = 1.1$ volts.

The only other parameters needed for the simulation were α_{sens} and k_{sens} for our tactile sensor, which we estimated using a recursive least squares method implemented in SciPy [28]. For this estimation, we used actual measurements from one trial with a pine wood block, resulting in $\alpha_{sens} = 2.796 * 10^{-9}\ m^2/s$ and $k_{sens} = 0.0349\ W/(mK)$.

To perform the simulation, we found the initial temperature of the sensor $T_{sens(t=0)}$ using eq. (2) and the surface temperature T_{surf} using eq. (3). We then computed $T_{sens(x=8*10^{-5},t)}$ using eq. (5). When compared with the average measurements from 60 real trials with wood and 60 real trials with aluminum, the pine wood simulation had an RMSE of 0.77°C, and the aluminum simulation had an RMSE of 1.08°C (see Fig. 8).

B. Model-based Inference

In this section, we use the model from Section IV to recognize an unknown material given consistent initial conditions based on a time-series of real temperature measurements from our tactile sensor, $T_{sens}(x = 8*10^{-5}, t)$. We use the model to estimate the material's thermal effusivity, e, at each point in time, where $e = \frac{k_{obj}}{\sqrt{\alpha_{obj}}}$. These estimates tend to improve with a longer duration of contact (see Fig. 9). To estimate e, we first find the sensor temperature just before contact, $T_{sens(t=0)}$.

$$T_{sens(t=0)} = \frac{\left(\frac{\dot{q}_x}{A}l + T_{amb}\right)}{k_{sens}} \tag{9}$$

based on eq. (9) with T_{amb} set to the currently measured ambient temperature and the other parameters set to the values described in Section V-A. We then combine eqs. (5) and (3) to find

$$e = \frac{T_{surf}\frac{k_{sens}}{\sqrt{\alpha_{sens}}} - T_{sens(t=0)}\frac{k_{sens}}{\sqrt{\alpha_{sens}}}}{T_{obj(t=0)} - T_{surf}} \tag{10}$$

where

$$T_{surf} = \frac{T_{sens}(x = 8 * 10^{-5}, t) - T_{sens(t=0)}}{erfc\left(\frac{8*10^{-5}}{2\sqrt{\alpha_{sens}t}}\right)} + T_{sens(t=0)}. \tag{11}$$

Notably, all of the terms in the resulting equation are constants, except for t and $T_{sens}(x = 8*10^{-5}, t)$. Consequently, we can use this equation to estimate the material's thermal effusivity, e, at each point in time using only the current time, t, and the current sensor temperature, $T_{sens}(x = 8 * 10^{-5}, t)$. To recognize a material, our algorithm compares these thermal effusivity estimates to values from the CES materials database [26]. For this paper, our algorithm used a 10-bin histogram of $\log_{10}(e)$ from the estimates made during a trial. It then found the bin containing the largest number of estimates and compared the range associated with this bin to the ranges associated with the candidate materials, as determined by the materials database. It then classifies the material as being the candidate material with the most similar range of values.

We evaluated this model-based method of material recognition using time series of raw temperature measurements from 60 trials with aluminum and 60 trials with pine wood using consistent initial conditions with substantial time between trials. Fig. 9 shows the results of plotting $\log_{10}(e)$ for all the estimates of e from these 120 trials. The top figure illustrates how the estimates change with duration of contact. The bottom figure shows a histogram produced from these values along with the ranges for aluminum and pine wood from the materials database. When using this method to recognize whether each of the 120 trials was pine wood versus aluminum, it had no errors and achieved 100% accuracy. However, this performance must be considered with caution, given the consistent initial conditions, the long duration of contact, and the very distinct thermal properties of aluminum and pine wood.

Given these results, model-based methods for material classification based on heat transfer merit further research. Perhaps more importantly, this model can potentially provide intuition for the estimation problem, inform feature selection, inform sensor design, and be used to generate synthetic data for evaluation and training. A clear benefit of this model-based method is that it can directly use information from materials databases. A potential limitation of this particular model-based method is that it is deterministic and does not represent various sources of uncertainty that could be relevant to the estimation.

VI. Data-driven Inference

In addition to our model-based method for inference, we evaluated three data-driven machine-learning algorithms that categorize materials based on the raw temperature and estimated slope over time. We chose these algorithms based on their wide usage and suitability for time series.

A. k-Nearest Neighbors and Support-Vector Machines

We implemented both k-nearest neighbors (k-NN) and support vector machines (SVMs) using the scikit-learn package [29] in Python. For k-NN we used k=3. For the SVMs, we used the svm.SVC() function, which performs multiclass classification using SVMs. This function implements multiclass classification via pairwise coupling as described in [30]. We used a linear kernel after trying other kernels, such as radial basis functions.

To produce feature vectors for training, we truncated the raw temperature time series to 500 samples, starting from the onset of contact, to produce a 500-dimensional feature vector. Due to the 200 Hz sampling rate, this resulted in approximately 2.5 s of data. When using both the raw temperature and the estimated slope, we truncated each time series to 500 samples from the onset of contact and concatenated them into a 1000-dimensional feature vector. To reduce the effect of noise and overfitting, we computed a low-dimensional representation of the training data with principal component analysis (PCA) before classification with k-NN or SVMs. In our classification experiments, we used 10 principal components for dimensionality reduction. 10 principal components could account for 95% of the variance of the 1000-dimensional feature vectors resulting from 5500 trials.

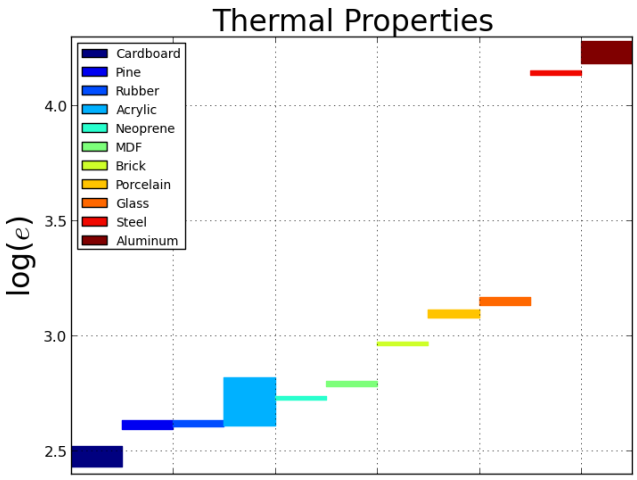

Fig. 10: *Thermal properties of materials used for experiments. Each material has a minimum and maximum value for* $\log(e)$. *The values are taken from CES materials database [26].*

B. Hidden Markov Model

We used a hidden Markov model (HMM) for each candidate material. We used multivariate continuous left-right HMMs with 25 hidden states and either 1 or 2 dimensional Gaussian emissions. We implemented them using the GHMM toolkit [31] in Python. We decided on these specifications based on results with preliminary data. We trained these HMMs with the standard Baum-Welch algorithm. For testing, we ran the Viterbi algorithm to find the HMM with the most probable state sequence given the observations and classified the material as being the material associated with this HMM [32].

VII. Experimental Results

In this section, we present our results from evaluating the three data-driven methods.

A. Consolidated Results

Fig. 10 shows the range of values of $\log(e)$ for the materials in our experiments based on the CES materials database [26]. As seen from the figure, some of the materials have overlapping ranges, while others are quite different.

Table I shows the consolidated results from our evaluation of the three data-driven algorithms using 3-fold cross-validation with 5500 trials (500 trials for each of the 11 materials). SVM+PCA outperformed the other algorithms. HMMs had the worst performance, confusing neoprene with pine wood and aluminum with steel.

TABLE I: Performance Summary.

Experimental Conditions	Features	HMMs	k-NN + PCA	SVM + PCA
Varied Initial Conditions and Contact Duration	One Feature	59.55%	82%	99%
	Two Features	53.2%	86%	99%

TABLE II: Effect of Initial Conditions.

Experimental Conditions	Data-driven Approach				Model based Approach
	Features	HMMs	k-NN + PCA	SVM + PCA	
Same Initial Conditions	One Feature	100%	100%	100%	100%
	Two Features	68.12%	100%	100%	

TABLE III: Effect of Contact Duration.

Experimental Conditions	Time (s)	HMMs	k-NN + PCA	SVM + PCA
Varied Initial Conditions	0.5	22.35%	63%	84%
	1.5	25.67%	77%	98%
	2.5	31.25%	82%	99%

B. Effect of Initial Conditions

We conducted another evaluation using 60 trials each for aluminum and pine wood with similar initial conditions. We extracted the features and ran all the algorithms for these 120 trials. Table II shows the results. The overall results are much better than with the randomized initial conditions. SVM+PCA, k-NN+PCA, and the model-based inference method (Section V-B) outperformed HMMs.

C. Effect of Contact Duration

To analyze the effect of contact duration on classification performance, we truncated the data at different time lengths and ran the algorithms. Table III shows the results (500 trials for each of the 11 materials). As expected, with increased length of the time, the performance of the algorithms improves. With 2.5 s of random and uncertain data, SVM+PCA reached an accuracy of 99%. When the input was reduced to 0.5 s of data, SVM+PCA achieved 84% accuracy.

D. Effect of Ambient Temperature

We also conducted a set of experiments wherein we varied the ambient temperature to see if our results would generalize. We performed this set of experiments in a similar manner to the first set of experiments with short-duration contact and varying initial conditions. Table IV shows the results (500 trials for aluminum and for pine wood). The overall trend remains the same and SVM+PCA shows the best cross-validation results with raw temperatures. However, the performance at higher temperature degrades when compared to the results at 25°C due to the smaller difference between the sensor's temperature and the material's temperature.

TABLE IV: Effect of Ambient Temperature.

Experimental Conditions	Ambient Temperature	HMMs	k-NN + PCA	SVM + PCA
Varied Initial Conditions and Contact Duration	25°C	83.2%	100%	100%
	35°C	66.4%	94%	91%

E. A Heat Generating Material (Human Skin)

We recruited 1 able-bodied participant via word of mouth. We obtained written informed consent from the participant according to our experimental protocol that was approved by the Institutional Review Board of the Georgia Institute of Technology. We collected 35 random initial condition trials on the forearm of the participant as shown in Fig. 2. The skin was at approximately 30°C and the ambient temperature was 26°C. The sensor was at 2° to 6°C above the forearm skin temperature just before contact. The experimental data presented in [33] indicates that the thermal conductivity of human skin is around $0.37 W/mK$. According to [26], out of the 11 materials we used in our other trials, MDF has the closest thermal conductivity to that of human-arm skin. We evaluated how well our best performing algorithm (SVM+PCA) could distinguish them. The algorithm successfully classified the two materials with 99% accuracy using raw temperatures and with 100% accuracy using both raw temperatures and slope estimates.

VIII. Conclusion

We investigated the classification of different materials based on heat transfer with short-duration contact and varying initial conditions. We conducted five sets of experiments using our 1-DOF experimental setup and implemented both model-based and data-driven methods for classification. We modeled the heat transfer between the sensor and the material as contact between two semi-infinite solids and used this model to categorize materials from temperature data. In addition to this model-based approach, we compared three data-driven algorithms for classification performance and found that SVM+PCA gave the best results. We also investigated the effect of initial conditions, contact duration, and ambient temperature on the classification algorithms' performance. Our results provide evidence for the feasibility of material classification by robots based on measurements acquired during short-duration contact with varying initial conditions. The performance of these methods during real-world tasks for which the contact between the sensor and the object is more varied, and there are greater numbers and varieties of objects, merits further inquiry.

IX. Acknowledgments

This work was supported by the National Science Foundation (NSF) Emerging Frontiers in Research and Innovation (EFRI) award 1137229 and NSF award IIS-1150157. We thank Prof. Melissa Kemp for valuable feedback and technical discussions, Phillip Grice for assistance with our human-subject research, the participant in our study, and the reviewers.

References

[1] T. Bhattacharjee, A. Kapusta, J. M. Rehg, and C. C. Kemp. Rapid categorization of object properties from incidental contact with a tactile sensing robot arm. In *IEEE-RAS International Conference on Humanoid Robots (Humanoids)*, October 2013.

[2] T. Bhattacharjee, P. M. Grice, A. Kapusta, M. D. Killpack, D. Park, and C. C. Kemp. A robotic system for reaching in dense clutter that integrates model predictive control, learning, haptic mapping, and planning. In *Proceedings of the 3rd IEEE/RSJ International Conference on Intelligent Robots and Systems (IROS) Workshop on Robots in Clutter: Perception and Interaction in Clutter*, 2014.

[3] P. M. Grice, M. D. Killpack, A. Jain, S. Vaish, J. Hawke, and C. C. Kemp. Whole-arm tactile sensing for beneficial and acceptable contact during robotic assistance. In *13th International Conference on Rehabilitation Robotics (ICORR)*, 2013.

[4] R. A. Russell. Thermal sensor for object shape and material constitution. *Robotica*, 6(01):31–34, 1988.

[5] R. A. Russell. A thermal sensor array to provide tactile feedback for robots. *The International journal of robotics research*, 4(3):35–39, 1985.

[6] D. Siegel, I. Garabieta, and J. M. Hollerbach. An integrated tactile and thermal sensor. In *Robotics and Automation. Proceedings. 1986 IEEE International Conference on*, volume 3, pages 1286–1291. IEEE, 1986.

[7] G. J. Monkman and P. M. Taylor. Thermal tactile sensing. *Robotics and Automation, IEEE Transactions on*, 9(3): 313–318, 1993.

[8] J. Engel, N. Chen, C. Tucker, C. Liu, S. Kim, and D. Jones. Flexible multimodal tactile sensing system for object identification. In *Sensors, 2006. 5th IEEE Conference on*, pages 563–566. IEEE, 2006.

[9] J. Engel, J. Chen, Z. Fan, and C. Liu. Polymer micromachined multimodal tactile sensors. *Sensors and Actuators A: Physical*, 117(1):50–61, 2005.

[10] Y. J. Yang, M. Y. Cheng, S. C. Shih, X. H. Huang, C. M. Tsao, F. Y. Chang, and K. C. Fan. A 32$\times$ 32 temperature and tactile sensing array using pi-copper films. *The International Journal of Advanced Manufacturing Technology*, 46(9-12):945–956, 2010.

[11] F. Castelli. An integrated tactile-thermal robot sensor with capacitive tactile array. In *Industry Applications Conference, 1995. Thirtieth IAS Annual Meeting, IAS'95., Conference Record of the 1995 IEEE*, volume 3, pages 1970–1975. IEEE, 1995.

[12] N. E. Mathis. New transient non-destructive technique measures thermal effusivity and diffusivity. *Thermal Conductivity*, 25:3–14, 2000.

[13] C. H. Lin, T. W. Erickson, J. A. Fishel, N. Wettels, and G. E. Loeb. Signal processing and fabrication of a biomimetic tactile sensor array with thermal, force and microvibration modalities. In *Robotics and Biomimetics (ROBIO), 2009 IEEE International Conference on*, pages 129–134. IEEE, 2009.

[14] D. G. Caldwell and J. O. Gray. dynamicmulti-functional tactile sensing. In *RoManSy 9*, pages 187–198. Springer, 1993.

[15] P. Mittendorfer and G. Cheng. Humanoid multimodal tactile-sensing modules. *Robotics, IEEE Transactions on*, 27(3):401–410, 2011.

[16] J. I. Yuji and K. Shida. A new multifunctional tactile sensing technique by selective data processing. *Instrumentation and Measurement, IEEE Transactions on*, 49 (5):1091–1094, 2000.

[17] D. Xu, G. E. Loeb, and J. A. Fishel. Tactile identification of objects using bayesian exploration. In *Robotics and Automation (ICRA), 2013 IEEE International Conference on*, pages 3056–3061. IEEE, 2013.

[18] I. McMahon, V. Chu, L. Riano, G.C. McDonald, Q. He, J.M. Perez-Tejada, M. Arrigo, N. Fitter, J. Nappo, T. Darrell, and K.J. Kuchenbecker. Robotic learning of haptic adjectives through physical interaction. In *Proceedings of the 2012 Second Workshop on Advances in Tactile Sensing and Touch-based Human-Robot Interaction*, 2012.

[19] S. Takamuku, T. Iwase, and K. Hosoda. Robust material discrimination by a soft anthropomorphic finger with tactile and thermal sense. In *Intelligent Robots and Systems, 2008. IROS 2008. IEEE/RSJ International Conference on*, pages 3977–3982. IEEE, 2008.

[20] E. Kerr, T. M. McGinnity, and S. Coleman. Material classification based on thermal properties-a robot and human evaluation. In *Robotics and Biomimetics (ROBIO), 2013 IEEE International Conference on*, pages 1048–1053. IEEE, 2013.

[21] Flexible Polyimide Foil Heater with 10 kOhm Thermistor. https://www.thorlabs.com/thorproduct.cfm?partnumber=HT10K.

[22] N. Mathis and C. Chandler. Direct thermal conductivity measurement technique, January 13 2004. URL http://www.google.com/patents/US6676287. US Patent 6,676,287.

[23] A. Maqsood, N. Amin, M. Maqsood, G. Shabbir, A. Mahmood, and S. E. Gustafsson. Simultaneous measurements of thermal conductivity and thermal diffusivity of insulators, fluids and conductors using the transient plane source (tps) technique. *International journal of energy research*, 18(9):777–782, 1994.

[24] Y. He. Rapid thermal conductivity measurement with a hot disk sensor: Part 1. theoretical considerations. *Thermochimica acta*, 436(1):122–129, 2005.

[25] Yunus C. and Afshin G. Transient heat conduction. In *Heat and Mass Transfer: Fundamentals and Applications*, chapter 4, pages 245–246. McGraw-Hill, New York, NY, 2010.

[26] M. F. Ashby. The ces edupack database of natural and man-made materials, 2008.

[27] J. S. Steinhart and S. R. Hart. Calibration curves for thermistors. In *Deep Sea Research and Oceanographic*

Abstracts, volume 15, pages 497–503. Elsevier, 1968.

[28] E. Jones, T. Oliphant, and P. Peterson. Scipy: Open source scientific tools for python. *http://www. scipy. org/*, 2001.

[29] F. Pedregosa, G. Varoquaux, A. Gramfort, V. Michel, B. Thirion, O. Grisel, M. Blondel, P. Prettenhofer, R. Weiss, V. Dubourg, J. Vanderplas, A. Passos, D. Cournapeau, M. Brucher, M. Perrot, and E. Duchesnay. Scikit-learn: Machine learning in Python. *Journal of Machine Learning Research*, 12:2825–2830, 2011.

[30] Ting-Fan Wu, Chih-Jen Lin, and Ruby C Weng. Probability estimates for multi-class classification by pairwise coupling. *The Journal of Machine Learning Research*, 5:975–1005, 2004.

[31] General Hidden Markov Model Library. http://ghmm.org/.

[32] L. R. Rabiner. A tutorial on hidden markov models and selected applications in speech recognition. In A. Waibel and K. F. Lee, editors, *Readings in Speech Recognition*, pages 267–296. Kaufmann, San Mateo, CA, 1990.

[33] Tissue Properties. http://www.itis.ethz.ch/itis-for-health/tissue-properties/database.